

ITEM3D: Illumination-Aware Directional Texture Editing for 3D Models

Shengqi Liu^{1*}, Zhuo Chen^{1*}, Jingnan Gao¹, Yichao Yan^{1†}, Wenhan Zhu¹,
Xiaobo Li², Ke Gao², Jiangjiang Lyu², Xiaokang Yang¹,

¹ MoE Key Lab of Artificial Intelligence, Shanghai Jiao Tong University
² Alibaba Group

{lsqlsq, ningci5252, gjn0310, yichao, zhuwenhan823, xkyang}@sjtu.edu.cn
{xiaobo.lixb, gaoke.gao, jiangjiang.ljj}@alibaba-inc.com

Abstract

Texture editing is a crucial task in 3D modeling that allows users to automatically manipulate the surface materials of 3D models. However, the inherent complexity of 3D models and the ambiguous text description lead to the challenge in this task. To address this challenge, we propose ITEM3D, an illumination-aware model for automatic 3D object editing according to the text prompts. Leveraging the diffusion models and the differentiable rendering, ITEM3D takes the rendered images as the bridge of text and 3D representation, and further optimizes the disentangled texture and environment map. Previous methods adopt the absolute editing direction namely score distillation sampling (SDS) as the optimization objective, which unfortunately results in the noisy appearance and text inconsistency. To solve the problem caused by the ambiguous text, we introduce a relative editing direction, an optimization objective defined by the noise difference between the source and target texts, to release the semantic ambiguity between the texts and images. Additionally, we gradually adjust the direction during optimization to further address the unexpected deviation in the texture domain. Qualitative and quantitative experiments show that our ITEM3D outperforms the state-of-the-art methods on various 3D objects. We also perform text-guided relighting to show explicit control over lighting.

1 Introduction

Texture editing is an important task in 3D modeling that involves manipulating the surface properties of 3D models to create a visually fantastic and appealing appearance according to the user’s ideas. With the increasing applications of 3D models in entertainment and e-shopping, how to automatically generate and edit the texture of a 3D model without manual effort becomes an appealing task in the field of 3D vision. However, this task is challenging due to the complexity of 3D models and the special representation of the texture.

To sufficiently handle the above applications, it would be desirable if a texture editing method can fulfill the following aspects: 1) **Realism**: The generated textures should give rise to realistic and visually natural 2D images after rendering. It requires generative models to capture the complex patterns and materials present in the textures of the 3D model. 2) **Relighting**: The editing method should balance the relighting

ability that allows adjusting the lighting conditions of the 3D model to be consistent with the changes made to its texture. 3) **Efficiency**: This requires the use of fast and memory-efficient rendering method that offers a differentiable connection between the 3D representation and 2D images.

Recent advances have demonstrated the effectiveness of generative models in synthesizing high-quality appearance that are both visually pleasing and semantically meaningful. The use of generative adversarial networks (GANs) (Xian et al. 2018; Bergmann, Jetchev, and Vollgraf 2017; Sun et al. 2022; Chen et al. 2023b) has shown promising results in producing textures with intricate patterns and complex structures. Other approaches, such as texture synthesis via direct optimization (Efros and Leung 1999; Frühstück, Alhashim, and Wonka 2019; Sendik and Cohen-Or 2017; Zhou et al. 2018) or neural style transfer (Berkiten et al. 2017; Hertz et al. 2020; Wang et al. 2022b; Mertens et al. 2006), have also been explored for their ability to generate textures with specific artistic styles. However, the capacity of these models is still unable to meet the need of real-world applications, which requires high-quality and diverse textures. Meanwhile, recent researches (Chen et al. 2023a; Richardson et al. 2023; Metzger et al. 2022; Lin et al. 2022; Liu et al. 2023; Kwar et al. 2022; Meng et al. 2021) on the diffusion models have emerged as a powerful new family of generative methods, which achieve impressive generation results in natural images and videos, inspiring us to introduce the awesome power into the task of 3D modeling.

However, directly applying the diffusion model to 3D objects is a non-trivial task due to the following reasons. 1) **The gap between the 3D representation and natural images**. Existing diffusion models are typically trained with natural images, making the pre-trained diffusion model lack prior knowledge in the 3D domain. Moreover, due to the complexity of the 3D model, it would be difficult to jointly edit shape, appearance, and shading, sometimes leading to conflicts in optimization goals. Therefore, directly editing the 3D representation may cause extreme semantic bias and sacrifice of inherent 3D topology. 2) **The learning misdirection of text description**. It is hard for text prompts to exactly describe the target images at the pixel level, leading to an ambiguous direction when taking the rendered images as the bridge.

To solve these problems, we present an efficient model, dubbed ITEM3D, which can generate visually natural texture

*These authors contributed equally.

†Corresponding authors

corresponding to the text prompt provided by users. Instead of directly applying the diffusion model for texture editing in the 2D space, we adopt rendered images as the intermediary that bridges the text prompts and the appearance of 3D models. Apart from the appearance, the lighting and shading are also key components influencing the rendering results. Therefore, we represent the 3D model into a triangular mesh, a set of disentangled materials consisting of the texture, and an environment map following nvdiffrac (Munkberg et al. 2022), which accomplishes the simultaneous modeling of both appearance and shading.

To optimize a texture and an environment map with the diffusion model, a naive idea is to adopt the score distillation sampling (SDS) like previous diffusion-based editing methods, which represents the absolute direction. Unfortunately, the utilization of absolute direction, such as SDS, often leads to noisy details and an inconsistent appearance, due to the ambiguous description of the text prompt for the target images. Inspired by the recent improvement (Hertz, Aberman, and Cohen-Or 2023), we replace the absolute editing direction led by the score distillation sampling with a relative editing direction determined by two predicted noises under the condition of the source text and the target text respectively, as illustrated in Fig. 1 (a). In this way, our model enables us to edit the texture in obedience to the text while bypassing the inconsistency problem by releasing the ambiguous description. It is ideal that the intermediate states between the source and target text can give relatively accurate descriptions for arbitrary rendered images during the optimization, like the green straight lines in Fig. 1 (b). However, the optimization in the texture domain actually shows the nonlinear distortion of the appearance in rendered images, leading to the deviation from the determined direction, like the red line in Fig. 1 (b). To reduce the deviation caused by the texture projection, we gradually adjust the editing direction during the optimization, as green fold lines shown in Fig. 1 (b). With the advent of the textural-inversion model, it can be easy to automatically correct the description as the change of the texture and its rendered images.

Thanks to the proposed solutions, our method overcomes the challenges of domain gap and learning misdirection, fulfilling all three requirements of texture editing. In summary, our contributions are:

- We design an efficient optimization pipeline to edit the texture and environment map obedient to the text prompt, directly empowering the downstream application in the industrial pipeline.
- We introduce the relative direction to the optimization of textured 3D model, releasing the problem of noisy details and inconsistent appearance caused by the semantic ambiguity between the texts and images.
- We propose to gradually adjust the relative direction guided by the source and target texts which addresses the unexpected deviation from the determined direction caused by the nonlinear texture projection.

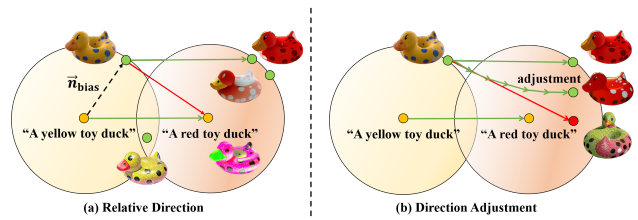


Figure 1: **Motivation.** (a) Previous methods (Poole et al. 2022; Chen et al. 2023a) with SDS Loss to directly guide the optimization leads to ambiguous details due to the bias between texts and images (red line), while our method introduces the relative direction between source and target texts to the optimization process, eliminating the bias and improving the rendering results (green line). (b) The optimization in the texture domain gives rise to the deviation of the target direction (red line), thus we gradually adjust the direction to fine-tune the optimization (fold green line).

2 Related Work

2.1 3D Model Representation

Neural Radiance Field. Neural implicit representations employ differentiable rendering techniques to reconstruct 3D geometry along with its corresponding appearance from multi-view images. Neural Radiance Field (NeRF) (Mildenhall et al. 2020) and followup approaches (Zhang et al. 2020; Wang et al. 2021b; Müller et al. 2022; Chen et al. 2022; Wizarawongsa et al. 2021; Yu et al. 2021; Reiser et al. 2021; Martin-Brualla et al. 2020) utilize volumetric representations and a neural encoder to compute radiance field. These methods explicitly represent the specular reflection as the appearance embedding on the surface, enabling the generation of high-fidelity rendering results. While these approaches are capable of capturing complex view-dependent appearances, they often suffer from poor surface reconstruction and limited relighting capabilities. To maintain the geometry quality, surface-based methods (Oechsle, Peng, and Geiger 2021; Wang et al. 2021a; Fu et al. 2022) introduce an implicit surface to the volumetric representation, resulting in improved geometry compared to pure NeRF-based methods. Nevertheless, these representations require excessive computation resources and still face challenges in disentangling material components for illumination-aware editing.

Neural inverse rendering. To solve the aforementioned problem, another category of methods focuses on the decomposition of rendering parameters. These methods introduce inverse rendering to estimate surface, materials, and lighting conditions simultaneously, achieving material editing and scene relighting. NeRV (Srinivasan et al. 2021) and NeRD (Boss et al. 2021) decompose the scene into the shape, reflectance and illumination components, enabling rendering under varying lighting conditions. NeRFactor (Zhang et al. 2021) introduces a two-stage method to separately reconstruct geometry and reflectance, simplifying reflectance optimization. Nvdiffrac (Munkberg et al. 2022) additionally introduces a differentiable model of environment lighting to efficiently recover all-frequency lighting. Leveraging the

decomposed explicit representation, our proposed method, ITEM3D, enables text-guided texture editing while preserving topology by design. Moreover, ITEM3D employs an efficient differentiable rasterization pipeline, further enhancing rendering efficiency.

2.2 3D Text-guided Generation

CLIP-based Generation. With the advent of large text-image models, CLIP, recent works (Wang et al. 2022a; Jetchev 2021; Jain et al. 2022; Michel et al. 2022) have led to impressive progress in 3D text-driven synthesis. The majority of methods adopt optimization procedures supervised by the CLIP similarity (Radford et al. 2021). Specifically, CLIP-NeRF (Wang et al. 2022a) proposes a unified framework to manipulate NeRF, guided by either a text prompt or an example image. Similarly, CLIP-Mesh utilizes an explicit textured mesh as a 3D representation, allowing for shape deformation along with corresponding texture modifications based on the input text. As the 3D-aware GAN gains popular, several works (Gal et al. 2022a; Chen et al. 2023b; Kim and Chun 2023) focus on the 3D stylization by fine-tuning the 3D GAN under the guidance of the CLIP model. However, the main drawback of CLIP-guided generation is the lack of diversity due to the deterministic embedding of the target prompt.

Diffusion-based Generation. Apart from the CLIP-based method, the diffusion model (Ho, Jain, and Abbeel 2020) has recently inspired huge breakthroughs in 3D text-guided generation. Dreamfusion (Poole et al. 2022) initially proposed the SDS loss as a means to incorporate the 2D prior of Stable Diffusion (Rombach et al. 2022) into the generation of 3D domains. Following Dreamfusion, Make-it-3D (Tang et al. 2023) incorporates the SDS loss to directly optimize NeRF and further refines the results using a texture point cloud. For general object synthesis, TEXTure (Richardson et al. 2023) employs an iterative scheme to paint a 3D model from different viewpoints based on a pre-trained depth-to-image diffusion model. Fantasia3D (Chen et al. 2023a) leverages the disentangled modeling and learns the geometry and appearance supervised by the score distillation sampling. However, these SDS-based methods often produce non-detailed and blurry outputs due to noisy gradients. In contrast, our ITEM3D utilizes the relative direction to eliminate the semantic ambiguity of the target prompt towards the texture. Recently, DreamBooth3D (Raj et al. 2023) and Instruc-NeRF2NeRF (Haque et al. 2023) utilize 2D diffusion to update the training images and fine-tune the NeRF training. While their models can achieve high-quality rendering results, the training process is too lengthy as they need an updating strategy to maintain the 3D consistency of NeRF representation during the editing process. In contrast, the decomposed 3D representation of our ITEM3D empowers us to directly optimize the texture and environment map, which significantly improves the training efficiency.

3 Method

3.1 Overview

Given a set of multi-view images $\mathcal{I} = \{I_1, \dots, I_n\}$, we first reconstruct the 3D model with both geometry and texture, and then edit the texture under the guidance of text prompts. To this end, we design a zero-shot differentiable framework that optimizes the disentangled materials of the object, *i.e.*, texture map and environment map. We leverage a differentiable rendering model to represent the 3D model as an accurate shape and surface materials with texture and environment map (Sec. 3.2). For further editing of appearance, we utilize the diffusion model to guide the direction of the texture optimization given the target text prompt. To solve the problem of ambiguous and noisy details, we introduce the relative direction of source text and target text into the optimization (Sec. 3.3). Moreover, we gradually adjust relative direction to address the challenges of deviation caused by the unbalanced optimization in the texture domain (Sec. 3.4). The overview of our method is demonstrated in Fig. 2.

3.2 3D Model Representation

To accomplish disentangled editing, we decompose the 3D model into a triangular mesh, a set of spatially varying materials and an environment map. The material model we employ, denoted as (k_d, k_{orm}, n) , combines a diffuse term k_d , a specular term k_{orm} , and a normal term n following the physically-based (PBR) material model introduced by Disney (Burley and Studios 2012). This PBR material model can be seamlessly integrated into existing industry rendering engines without any change.

Additionally, for efficient representation of volumetric textures, we leverage a multi-layer perceptron (MLP) to encode all material parameters into a compact representation. Specifically, given a world space position x , we compute the MLP texture, which includes the base color, k_d , the specular parameters k_{orm} , and a tangent space normal perturbation n . This mapping is formulated as $x \rightarrow (k_d, k_{orm}, n)$. With the introduction of MLP texture representation, the textures are initialized by sampling the MLP on the mesh surface and then optimized efficiently, while maintaining a fixed topology.

Following the rendering equation of the image-based lighting model, we integrate all the incoming radiance $L_i(\omega_i)$ from the environment map and compute the outgoing radiance L in direction ω_o using the following equation:

$$L(\omega_o) = \int_{\Omega} L_i(\omega_i) f(\omega_i, \omega_o) (\omega_i \cdot \mathbf{n}) d\omega_i, \quad (1)$$

where the $f(\omega_i, \omega_o)$ represents the BSDF function, and the integration domain is the hemisphere Ω around the intersection normal n . For real-time rendering, we employ the split-sum approximation (Karis and Games 2013) and the integral radiance in Eq. (1) is approximated as:

$$L(\omega_o) \approx \int_{\Omega} f(\omega_i, \omega_o) (\omega_i \cdot \mathbf{n}) d\omega_i + \int_{\Omega} L_i(\omega_i) D(\omega_i, \omega_o) (\omega_i \cdot \mathbf{n}) d\omega_i. \quad (2)$$

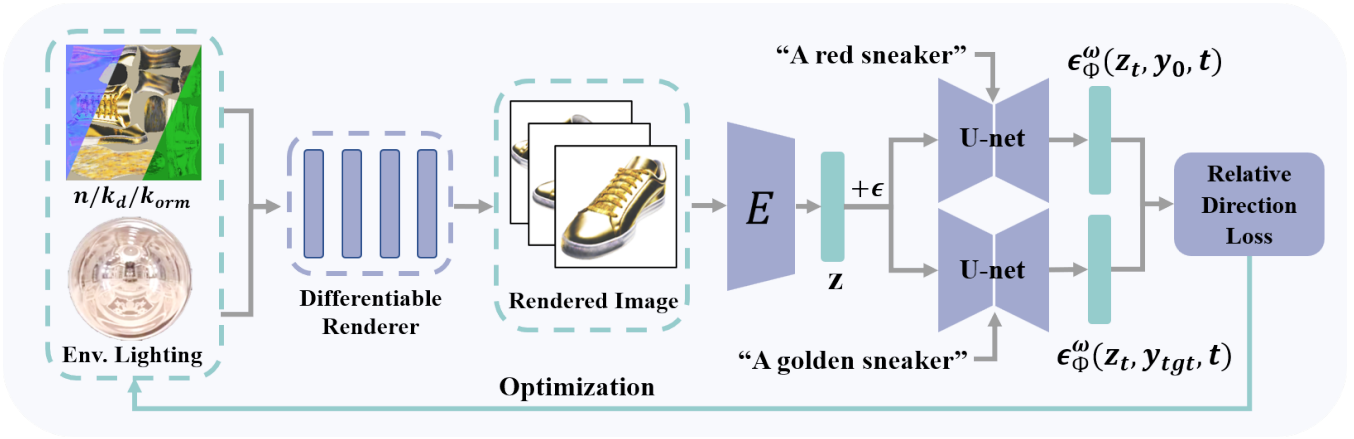


Figure 2: **Pipeline** of 3D model editing. We render the 3D model with mesh, texture, and environment map into 2D images which are then added with noise ϵ . We further separately use the source text and the target text as the conditions to predict the added noise via the U-Net. The difference between the two predicted noises serve as the relative direction to guide the optimization of the materials and environment map.

The first term of this product only relies on the parameters $(\omega_i \cdot \mathbf{n})$ and the roughness r of the BSDF $f(\omega_i, \omega_o)$, which is precomputed and stored in a 2D lookup texture. Meanwhile, the second term is the integral of the incident radiance with the GGX (Walter et al. 2007) normal distribution D , which is also precomputed and stored by a filtered cubemap following Karis (Karis and Games 2013).

In order to learn the environment lighting from 2D image observations, we employ a differentiable split sum shading model. We represent the environment light as a high-resolution cube map, which is the trainable parameters in the shading model. Owing to the precomputation and lookup mechanism, the rendering process from the texture/normal/environment map to the 2D images can be greatly accelerated. This approach serves as a bridge that allows ITEM3D to directly optimize the texture and environment map through rendered 2D images, rather than optimizing the complex 3D representation. As a result, the number of parameters to be optimized is significantly reduced, leading to a more efficient editing process.

3.3 Relative Direction Based Optimization

To enable the appearance editing of 3D models using natural language, a direct idea is to utilize the diffusion model that has been pre-trained in 2D images as knowledge prior. Naively, we can use Score Distillation Sampling (SDS) loss,

$$\nabla_{\theta} \mathcal{L}_{\text{SDS}}(\phi, \mathbf{x} = \mathcal{R}(\theta)) = \mathbb{E}_{t, \epsilon} \left[w(t) (\epsilon_{\phi}^{\omega}(\mathbf{z}_t; y, t) - \epsilon) \frac{\partial \mathbf{x}}{\partial \theta} \right], \quad (3)$$

where \mathbf{x} is the rendered images, t is the sampled time step, \mathbf{z}_t is the t time step latent, $w(t)$ is the weighting function that equals $\partial \mathbf{z}_t / \partial \mathbf{x}$, y is the text condition, $\epsilon_{\phi}^{\omega}(\mathbf{z}_t; y, t)$ is the predicted noise through classifier-free guidance, and $\epsilon \in N(0, I)$ is the noise added to the rendered images. The gradient of SDS loss gives an editing direction for our texture optimization, determined by the text prompt y . However, the SDS loss

may harm the content of original images with noisy details, because the text prior typically cannot faithfully reflect the information of the image. It is known that the entropy of an RGB image is significantly larger than that of a text prompt. As a consequence, the misdescription inevitably arises when taking the text prompt as the prior to restore the high-quality image from the same-scale noise. Therefore, even for a text prompt y_0 describing the original images, there exists a deviation related to the optimized texture θ between the added noise ϵ and the predicted noise $\epsilon_{\phi}^{\omega}(\mathbf{z}_t; y_0, t)$, which can be simply expressed as,

$$D_{\text{bias}}(\theta, \dots) \propto \|\epsilon_{\phi}^{\omega}(\mathbf{z}_t; y_0, t) - \epsilon\|. \quad (4)$$

Thus, the gradient leads to a bias term from the original input image, which can be expressed as,

$$\vec{n}_{\text{bias}} = \frac{\partial D_{\text{bias}}(\theta, \dots)}{\partial \theta} = (\epsilon_{\phi}^{\omega}(\mathbf{z}_t; y_0, t) - \epsilon) \frac{\partial \mathbf{x}}{\partial \theta}. \quad (5)$$

Moreover, for an arbitrary text prompt y_{tgt} describing the target editing texture, it could be considered that there exists a term of expected editing direction and a term of bias discussed above,

$$(\epsilon_{\phi}^{\omega}(\mathbf{z}_t; y_{\text{tgt}}, t) - \epsilon) \frac{\partial \mathbf{x}}{\partial \theta} = \vec{n}_{\text{tgt}} + \vec{n}_{\text{bias}}. \quad (6)$$

As a result, the \vec{n}_{bias} gives rise to the misdirection for the optimization procedure.

To address these issues, it is ideal to find the accurate editing direction \vec{n}_{tgt} , while the term of \vec{n}_{bias} is hard to estimate due to the diverse input images. To mitigate the gap, it is natural to take the text guidance as a relative direction rather than an absolute direction, enabling us to eliminate the term of \vec{n}_{bias} . The absolute direction of the source \vec{n}_{src} and the target \vec{n}_{tgt} can be expressed as,

$$\vec{n}_{\text{src}} = (\epsilon_{\phi}^{\omega}(\mathbf{z}_t; y_0, t) - \epsilon) \frac{\partial \mathbf{x}}{\partial \theta} - \vec{n}_{\text{bias}}, \quad (7)$$



Figure 3: **Performance on real-world objects.** The textured mesh is reconstructed from multi-view images, after which we employ the corresponding prompts to modify the textured mesh, showcasing our exceptional ability to edit real-world objects. ITEM3D successfully transform the original cat toy into a vegetable tiger toy, the piggy doll into a porcelain pig, and the sneaker into a golden sneaker with remarkable quality.

$$\vec{n}_{\text{tgt}} = (\epsilon_{\phi}^{\omega}(\mathbf{z}_t; y_{\text{tgt}}, t) - \epsilon) \frac{\partial \mathbf{x}}{\partial \theta} - \vec{n}_{\text{bias}}, \quad (8)$$

where \vec{n}_{src} is actually the $\vec{0}$ giving no extra information to the input images. Inspired by the CLIP-directional loss improved by the StyleGAN-Nada (Gal et al. 2022b) and the denoising loss proposed by the recent work (Poole et al. 2022), we utilize the difference between the source \vec{n}_{src} and the target \vec{n}_{tgt} as the relative direction of the target, which can be presented as,

$$\vec{n}_{\text{tgt}} = \vec{n}_{\text{tgt}} - \vec{n}_{\text{src}} = (\epsilon_{\phi}^{\omega}(\mathbf{z}_t; y_{\text{tgt}}, t) - \epsilon_{\phi}^{\omega}(\mathbf{x}, y_0, t)) \frac{\partial \mathbf{x}}{\partial \theta}. \quad (9)$$

Therefore, the final gradient utilized for optimizing the texture can be presented as,

$$\begin{aligned} \nabla_{\theta} \mathcal{L}_{\text{RDL}}(\phi, \mathbf{x} = \mathcal{R}(\theta)) = \\ \mathbb{E}_{t, \epsilon} \left[w(t) (\epsilon_{\phi}^{\omega}(\mathbf{z}_t; y_{\text{tgt}}, t) - \epsilon_{\phi}^{\omega}(\mathbf{z}_t; y_0, t)) \frac{\partial \mathbf{x}}{\partial \theta} \right], \quad (10) \end{aligned}$$

3.4 Direction Adjustment

Different from the gradual transition in the nature image domain, the optimization of the texture domain unfortunately shows an unexpected offset of the appearance in rendered images, due to the complex projection in differentiable rendering. The inherent reason is that the complexity of rendering leads to unbalanced optimization for the texture, with some parts under-tuning and other parts over-tuning. This appearance offset can be seen in some parts of the rendered image, leading to the inconsistency between the source text and the rendered images in the median period of the optimization procedure. It is known that a source image with an inconsistent text description means an optimization misdirection which leads to an unknown change in the editing results. Similar to the known problem, if a rendered image during the median optimization hops out the direction between the source text and the target text, it can be considered as the inconsistent description for the source image when we take the current median point as a relative beginning point. The

original editing direction is give by,

$$\vec{n}_{\text{ori}} = \vec{n}_{\text{tgt}} - \vec{n}_{\text{src}}. \quad (11)$$

If the optimization continues along the original direction, a more severe deviation can be attached to the optimization procedure.

To avoid the misdirection caused by the texture domain, we propose to adjust the editing direction, specifically changing the source text prompt gradually, during our optimization process of the texture map. The direction after adjustment $\Delta \hat{T}_i$ can be represented as,

$$\Delta \hat{T}_i = \vec{n}_i - \vec{n}_{i-1} = \mathcal{B}(I_i) - \mathcal{B}(I_{i-1}), \quad (12)$$

where i is the optimization iteration and $\mathcal{B}(\cdot)$ expresses the inverse text generated by a pre-trained language-image model BLIP-v2 (Li et al. 2023).

As shown in the Fig. 1 (b), the direction is continually adjusted during the optimization so that the new global direction \vec{n}_i can be written as,

$$\vec{n}_i = \vec{n}_{\text{ori}} + \sum_{j \leq i} \Delta \hat{T}_j. \quad (13)$$

By adjusting the optimization direction step by step, we achieve more delicate and controllable editing, which can be seen in Sec. 4.4.

4 Experiments

4.1 Implementation Details

Dataset. In the experiments, we mainly evaluate our model on the NeRF Synthetic (Mildenhall et al. 2020) dataset. The NeRF synthetic dataset consists of 8 path-traced scenes with multi-view images which we reconstruct into our textural mesh-based representation via nvdiffric (Munkberg et al. 2022). Besides, we also adopt 3D objects from Keenan’s 3D model repository and a set of real-world products to verify the ability of generalization.

Experiment Setup. We optimize the 3D model on one RTX A6000 GPU with 48G memory. The optimization procedure lasts about average 600 iterations with 10 minutes for each 3D model. We use the Adam optimizer for both the texture and the environment map with the learning rate of 0.01.

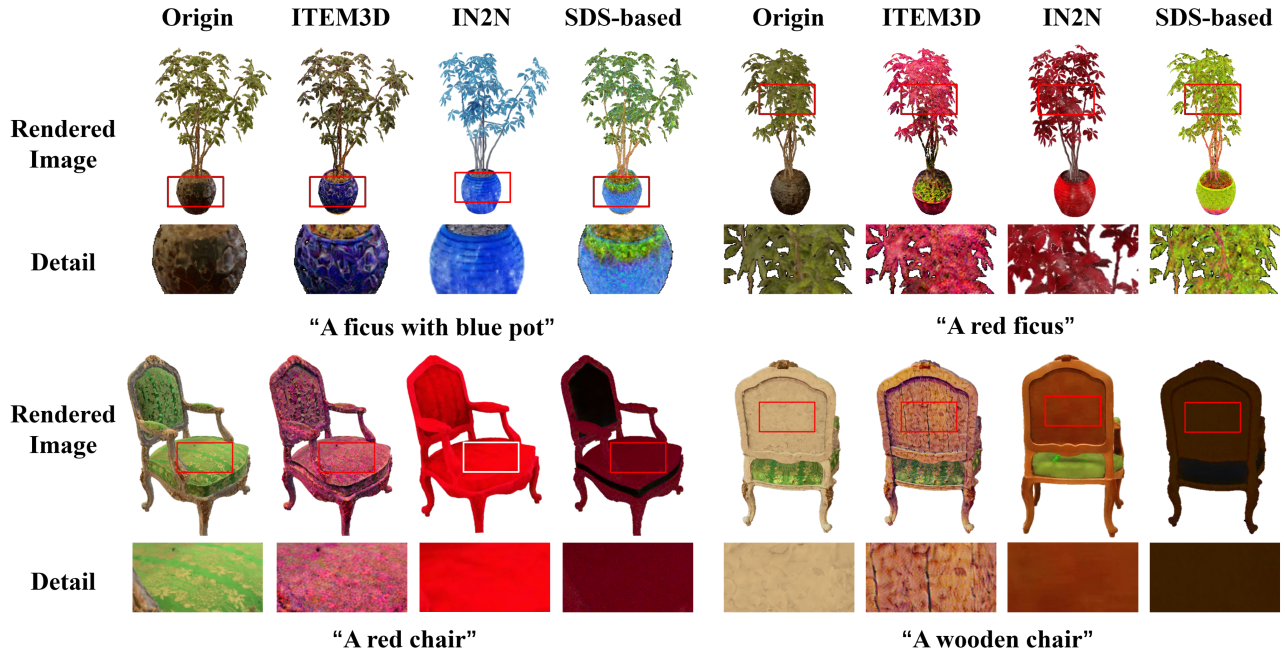


Figure 4: **Qualitative comparison** on NeRF synthetic dataset. We conducted a comparative analysis of our method with the state-of-the-art approach, Instruct-NeRF2NeRF (IN2N) and the simple SDS-based method. While both ITEM3D and IN2N demonstrate prompt-consistent editing, the SDS-based method fails to yield satisfactory outcomes. Conversely, IN2N exhibits a loss of the original chair patterns and an inability to faithfully represent natural wood patterns. Moreover, it lacks the necessary precision to accurately discern the edited object.

4.2 Qualitative Results.

Results on real dataset. We perform ITEM3D on a real-world dataset, and the results are depicted in Fig. 3. Our ITEM3D approach showcases remarkable texture editing capabilities for real products, including a shoe, a piggy doll, and a toy cat. For instance, when given the text prompt “a vegetable tiger toy”, ITEM3D effectively transforms the texture into that of a cute, furry tiger while preserving the structure of the original toy cat. Furthermore, when the prompts involve both material and texture descriptions, e.g., “a golden sneaker”, our model successfully bake the golden material instead of original material into the texture and show a realistic shoe. Similarly, the example of “a pink porcelain piggy toy” also achieves realistic material editing along with consistent texture modifications as the provided text. These results clearly demonstrate the generalization ability of ITEM3D in handling complex real-world objects.

Comparison on synthetic dataset. We conducted a comparative analysis among ITEM3D, SDS-based optimization method, and the state-of-the-art approach Instruct-NeRF2NeRF (IN2N), as shown in Fig. 4. While SDS-based method could edit textures along the direction of text prompt, its rendered images show unrealistic appearance and tend to overfit to the text. In contrast, ITEM3D and IN2N can render realistic images with high quality while remaining consistent with the input text prompt. However, IN2N has certain limitations in comparison to our approach. For instance, when editing chairs, IN2N produces results with less details

and smooth textures, lacking the fine grain that our method captures. Furthermore, when editing a ficus plant with the prompt “make it into a blue pot”, IN2N faces challenges in distinguishing between the pot and the plant, resulting in both elements being edited to the same blue color. The comparison indicates the effectiveness of the introduced relative direction of optimization and further direction adjustment.

4.3 Quantitative Results

Editing Quality. We conduct a quantitative comparison in the Tab. 1. To evaluate the semantic consistency, we render 512×512 RGB images after texture editing, and further compute the CLIP-Score of the rendered image and corresponding target text. CLIP-score contains two parts, *i.e.*, global score and directional score. Global score measures the similarity between the target text and the editing images, and directional score measures the similarity between two editing directions of text prompts and images, which are expressed as which can be presented as,

$$\text{Score}_{\text{global}} = \frac{T_{\text{tgt}} \cdot I_{\text{tgt}}}{\|T_{\text{tgt}}\| \|I_{\text{tgt}}\|}, \quad \text{Score}_{\text{direction}} = \frac{\Delta T \cdot \Delta I}{\|\Delta T\| \|\Delta I\|}, \quad (14)$$

where T_{tgt} and I_{tgt} are the embedding of target text and edited image encoded by the CLIP encoder, and ΔT and ΔI are expressed as,

$$\Delta T = T_{\text{tgt}} - T_{\text{src}}, \quad \Delta I = I_{\text{tgt}} - I_{\text{src}}. \quad (15)$$

As illustrated in Tab. 1, our method achieves better results than the SDS-based method and Instruct-NeRF2NeRF.

Table 1: **Quantitative Comparisons.** We report two CLIP-based scores, *i.e.*, global score and directional score to evaluate the semantic quality of rendered images. We also compared the editing time and memory consumption of three methods.

Method	ITEM3D	SDS-based	IN2N
Global Score \uparrow	0.35	0.30	0.33
Directional Score \uparrow	0.27	0.18	0.23
Training Time \downarrow	10min	8min	10h
GPU Memory \downarrow	9GB	9GB	15GB

Table 2: **User study** conducted with 33 participants. Each participant scores based on two evaluation criteria, *i.e.*, photorealism and text consistency. The range of scores is from 1 to 5, where 1 represents worst and 5 represents best.

Method	ITEM3D	SDS-based	IN2N
Photorealism \uparrow	3.98	2.77	3.82
Text Consistency \uparrow	4.11	2.45	4.02

Editing Efficiency. Moreover, to demonstrate the editing efficiency of ITEM3D, we compare the training time and GPU memory with Instruct-NeRF2NeRF in the Tab. 1. Our findings show that ITEM3D outperforms instruct-NeRF2NeRF, requiring significantly less time (50 times less) while maintaining less memory consumption during texture editing.

User Study. Additionally, we perform a user study in Tab. 2 to further assess the quality of editing objects. Users are required to rate on a scale of 1 to 5, based on the following questions: (1) Are the edited objects realistic and natural (Photorealism)? (2) Are the edited objects accurately reflect the target text’s semantics (Text Consistency)? As presented in Tab. 2, the results demonstrate the superior quality with higher realism and more text consistency of our proposed method as compared to the baselines.

4.4 Direction Adjustment

In this section, we further study the necessity of direction adjustment. We perform the ablation study in Fig. 5. Without the adjustment for the relative optimization direction, the texture shows a wired change that the duck gradually generates two heads and the color seems partially yellow and partially red. When applying the gradual adjustment, the duck bypasses the unnatural change and smoothly achieves the target appearance. The example of cattle shows a similar trend. In this experiment, it can be noticed that there exists unbalanced optimization for different parts of the texture. The optimization scheme of simple pieces of texture converges quickly, while more complex modifications require longer time, which in turn over-tunes easy parts leading to poor results.

4.5 Illumination-aware Editing

The disentangled representation of the environment map empowers ITEM3D to explicitly relight the 3D model. The results of illumination-aware editing are demonstrated in Fig. 6.



Figure 5: **Ablation study** of direction adjustment. The results without adjustment show a wired appearance, *i.e.*, pale body of the cattle and dual heads of the duck. When applying gradual adjustment, the unrealistic artifacts are released, in result of natural appearance.

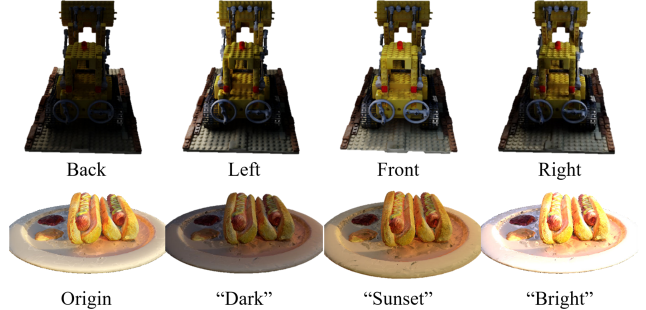


Figure 6: **Relighting results.** ITEM3D has capacity of explicit control over the lighting direction by manipulating the environment map. Furthermore, ITEM3D can relight the 3D model based on the text guidance via the optimization of disentangled environment map.

The Lego cases show the capability to modify the lighting direction by directly manipulating the environment map. Moreover, the hotdog cases showcase the ability to guide relighting using text prompts, while maintaining the texture constant. During the text-guided relighting, we fix the texture and mesh components and focus on optimizing the environment map based on provided text prompts, such as “dark”, “sunset” and “bright light”. It proves that the diffusion model can utilize the lighting prior information from 2D images to guide the optimization for the environment map by leveraging the differential rendering process.

5 Conclusion and Limitations

In conclusion, our ITEM3D model presents an efficient solution to the challenging task of texture editing for 3D models. By leveraging the knowledge from diffusion models, ITEM3D is capable to optimize the texture and environment map under the guidance of text prompts. To address the semantic ambiguity between text prompts and images, we replace the traditional score distillation sampling (SDS) with a relative editing direction. We further propose a gradual direction adjustment during the optimization procedure, solving the unbalanced optimization in the texture.

Despite the promising editing results, our ITEM3D still remains several limitations which should be solved in future work. The major limitation is that our method may encounter challenges when dealing with complex and precise editing

prompts. Another limitation is that it is hard to edit the lighting direction directly by the guidance of text prompt. Our further work aims to explore the learning scheme to solve the problem of unbalanced optimization in the texture.

References

- Bergmann, U.; Jetchev, N.; and Vollgraf, R. 2017. Learning Texture Manifolds with the Periodic Spatial GAN. In *ICML*, volume 70, 469–477.
- Berkiten, S.; Halber, M.; Solomon, J.; Ma, C.; Li, H.; and Rusinkiewicz, S. 2017. Learning Detail Transfer based on Geometric Features. *Comput. Graph. Forum*, 36(2): 361–373.
- Boss, M.; Braun, R.; Jampani, V.; Barron, J. T.; Liu, C.; and Lensch, H. 2021. NerD: Neural reflectance decomposition from image collections. In *ICCV*, 12684–12694.
- Burley, B.; and Studios, W. D. A. 2012. Physically-based shading at disney. In *Acm Siggraph*, volume 2012, 1–7.
- Chen, A.; Xu, Z.; Geiger, A.; Yu, J.; and Su, H. 2022. Tensorf: Tensorial radiance fields. In *ECCV*, 333–350.
- Chen, R.; Chen, Y.; Jiao, N.; and Jia, K. 2023a. Fantasia3D: Disentangling Geometry and Appearance for High-quality Text-to-3D Content Creation. *arXiv preprint arXiv:2303.13873*.
- Chen, Z.; Xu, X.; Yan, Y.; Pan, Y.; Zhu, W.; Wu, W.; Dai, B.; and Yang, X. 2023b. HyperStyle3D: Text-Guided 3D Portrait Stylization via Hypernetworks. *arXiv preprint arXiv:2304.09463*.
- Efros, A. A.; and Leung, T. K. 1999. Texture Synthesis by Non-parametric Sampling. In *ICCV*, 1033–1038.
- Frühstück, A.; Alhashim, I.; and Wonka, P. 2019. TileGAN: synthesis of large-scale non-homogeneous textures. *ACM Trans. Graph.*, 38(4): 58:1–58:11.
- Fu, Q.; Xu, Q.; Ong, Y. S.; and Tao, W. 2022. Geo-neus: Geometry-consistent neural implicit surfaces learning for multi-view reconstruction. *NeurIPS*, 35: 3403–3416.
- Gal, R.; Patashnik, O.; Maron, H.; Bermano, A. H.; Chechik, G.; and Cohen-Or, D. 2022a. Stylegan-nada: Clip-guided domain adaptation of image generators. *ACM Transactions on Graphics (TOG)*, 1–13.
- Gal, R.; Patashnik, O.; Maron, H.; Bermano, A. H.; Chechik, G.; and Cohen-Or, D. 2022b. StyleGAN-NADA: CLIP-guided domain adaptation of image generators. *ACM Trans. Graph.*, 41(4): 141:1–141:13.
- Haque, A.; Tancik, M.; Efros, A. A.; Holynski, A.; and Kanazawa, A. 2023. Instruct-nerf2nerf: Editing 3d scenes with instructions. *arXiv preprint arXiv:2303.12789*.
- Hertz, A.; Aberman, K.; and Cohen-Or, D. 2023. Delta Denoising Score. *arXiv preprint arXiv:2304.07090*.
- Hertz, A.; Hanocka, R.; Giryes, R.; and Cohen-Or, D. 2020. Deep geometric texture synthesis. *ACM Trans. Graph.*, 39(4): 108.
- Ho, J.; Jain, A.; and Abbeel, P. 2020. Denoising diffusion probabilistic models. *NeurIPS*, 33: 6840–6851.
- Jain, A.; Mildenhall, B.; Barron, J. T.; Abbeel, P.; and Poole, B. 2022. Zero-shot text-guided object generation with dream fields. In *CVPR*, 867–876.
- Jetchev, N. 2021. Clipmatrix: Text-controlled creation of 3d textured meshes. *arXiv preprint arXiv:2109.12922*.
- Karis, B.; and Games, E. 2013. Real shading in unreal engine 4. *Proc. Physically Based Shading Theory Practice*, 4(3): 1.
- Kawar, B.; Zada, S.; Lang, O.; Tov, O.; Chang, H.; Dekel, T.; Mosseri, I.; and Irani, M. 2022. Imagic: Text-based real image editing with diffusion models. *arXiv preprint arXiv:2210.09276*.
- Kim, G.; and Chun, S. Y. 2023. Datid-3d: Diversity-preserved domain adaptation using text-to-image diffusion for 3d generative model. In *CVPR*, 14203–14213.
- Li, J.; Li, D.; Savarese, S.; and Hoi, S. 2023. Blip-2: Bootstrapping language-image pre-training with frozen image encoders and large language models. *arXiv preprint arXiv:2301.12597*.
- Lin, C.; Gao, J.; Tang, L.; Takikawa, T.; Zeng, X.; Huang, X.; Kreis, K.; Fidler, S.; Liu, M.; and Lin, T. 2022. Magic3D: High-Resolution Text-to-3D Content Creation. *arXiv preprint arXiv:2211.10440*.
- Liu, R.; Wu, R.; Van Hoorick, B.; Tokmakov, P.; Zakharov, S.; and Vondrick, C. 2023. Zero-1-to-3: Zero-shot One Image to 3D Object. *arXiv preprint arXiv:2303.11328*.
- Martin-Brualla, R.; Radwan, N.; Sajjadi, M. S.; Barron, J. T.; Dosovitskiy, A.; and Duckworth, D. 2020. Nerf in the wild: Neural radiance fields for unconstrained photo collections. *arXiv preprint arXiv:2008.02268*.
- Meng, C.; Song, Y.; Song, J.; Wu, J.; Zhu, J.-Y.; and Ermon, S. 2021. Sdedit: Image synthesis and editing with stochastic differential equations. *arXiv preprint arXiv:2108.01073*.
- Mertens, T.; Kautz, J.; Chen, J.; Bekaert, P.; and Durand, F. 2006. Texture Transfer Using Geometry Correlation. In *Proceedings of the Eurographics Symposium on Rendering Techniques*, 273–284.
- Metzer, G.; Richardson, E.; Patashnik, O.; Giryes, R.; and Cohen-Or, D. 2022. Latent-NeRF for Shape-Guided Generation of 3D Shapes and Textures. *arXiv preprint arXiv:2211.07600*.
- Michel, O.; Bar-On, R.; Liu, R.; Benaim, S.; and Hanocka, R. 2022. Text2mesh: Text-driven neural stylization for meshes. In *CVPR*, 13492–13502.
- Mildenhall, B.; Srinivasan, P. P.; Tancik, M.; Barron, J. T.; Ramamoorthi, R.; and Ng, R. 2020. Nerf: Representing scenes as neural radiance fields for view synthesis. In *ECCV*, 99–106.
- Müller, T.; Evans, A.; Schied, C.; and Keller, A. 2022. Instant neural graphics primitives with a multiresolution hash encoding. *ACM Transactions on Graphics (ToG)*, 41(4): 1–15.
- Munkberg, J.; Hasselgren, J.; Shen, T.; Gao, J.; Chen, W.; Evans, A.; Müller, T.; and Fidler, S. 2022. Extracting triangular 3d models, materials, and lighting from images. In *CVPR*, 8280–8290.
- Oechsle, M.; Peng, S.; and Geiger, A. 2021. UNISURF: Unifying Neural Implicit Surfaces and Radiance Fields for Multi-View Reconstruction. *arXiv preprint arXiv:2104.10078*.

- Poole, B.; Jain, A.; Barron, J. T.; and Mildenhall, B. 2022. DreamFusion: Text-to-3D using 2D Diffusion. *arXiv preprint arXiv:2209.14988*.
- Radford, A.; Kim, J. W.; Hallacy, C.; Ramesh, A.; Goh, G.; Agarwal, S.; Sastry, G.; Askell, A.; Mishkin, P.; Clark, J.; et al. 2021. Learning transferable visual models from natural language supervision. In *ICML*, 8748–8763.
- Raj, A.; Kaza, S.; Poole, B.; Niemeyer, M.; Ruiz, N.; Mildenhall, B.; Zada, S.; Aberman, K.; Rubinstein, M.; Barron, J.; et al. 2023. Dreambooth3d: Subject-driven text-to-3d generation. *arXiv preprint arXiv:2303.13508*.
- Reiser, C.; Peng, S.; Liao, Y.; and Geiger, A. 2021. KiloNeRF: Speeding up Neural Radiance Fields with Thousands of Tiny MLPs. *arXiv preprint arXiv:2103.13744*.
- Richardson, E.; Metzger, G.; Alaluf, Y.; Giryas, R.; and Cohen-Or, D. 2023. Texture: Text-guided texturing of 3d shapes. *arXiv preprint arXiv:2302.01721*.
- Rombach, R.; Blattmann, A.; Lorenz, D.; Esser, P.; and Ommer, B. 2022. High-resolution image synthesis with latent diffusion models. In *CVPR*, 10684–10695.
- Sendik, O.; and Cohen-Or, D. 2017. Deep Correlations for Texture Synthesis. *ACM Trans. Graph.*, 36(5): 161:1–161:15.
- Srinivasan, P. P.; Deng, B.; Zhang, X.; Tancik, M.; Mildenhall, B.; and Barron, J. T. 2021. Nerv: Neural reflectance and visibility fields for relighting and view synthesis. In *CVPR*, 7495–7504.
- Sun, J.; Wang, X.; Shi, Y.; Wang, L.; Wang, J.; and Liu, Y. 2022. IDE-3D: Interactive Disentangled Editing for High-Resolution 3D-Aware Portrait Synthesis. *ACM Trans. Graph.*, 41(6): 270:1–270:10.
- Tang, J.; Wang, T.; Zhang, B.; Zhang, T.; Yi, R.; Ma, L.; and Chen, D. 2023. Make-it-3d: High-fidelity 3d creation from a single image with diffusion prior. *arXiv preprint arXiv:2303.14184*.
- Walter, B.; Marschner, S. R.; Li, H.; and Torrance, K. E. 2007. Microfacet Models for Refraction through Rough Surfaces. In *Proceedings of the Eurographics Symposium on Rendering Techniques*, 195–206.
- Wang, C.; Chai, M.; He, M.; Chen, D.; and Liao, J. 2022a. Clip-nerf: Text-and-image driven manipulation of neural radiance fields. In *CVPR*, 3835–3844.
- Wang, P.; Liu, L.; Liu, Y.; Theobalt, C.; Komura, T.; and Wang, W. 2021a. NeuS: Learning Neural Implicit Surfaces by Volume Rendering for Multi-view Reconstruction. *arXiv preprint arXiv:2106.10689*.
- Wang, Z.; Wu, S.; Xie, W.; Chen, M.; and Prisacariu, V. A. 2021b. NeRF-: Neural radiance fields without known camera parameters. *arXiv preprint arXiv:2102.07064*.
- Wang, Z.; Zhao, L.; Chen, H.; Li, A.; Zuo, Z.; Xing, W.; and Lu, D. 2022b. Texture Reformer: Towards Fast and Universal Interactive Texture Transfer. In *AAAI*, 2624–2632.
- Wizadwongsa, S.; Phongthawee, P.; Yenphraphai, J.; and Suwajanakorn, S. 2021. Nex: Real-time view synthesis with neural basis expansion. In *CVPR*, 8534–8543.
- Xian, W.; Sangkloy, P.; Agrawal, V.; Raj, A.; Lu, J.; Fang, C.; Yu, F.; and Hays, J. 2018. TextureGAN: Controlling Deep Image Synthesis With Texture Patches. In *CVPR*, 8456–8465.
- Yu, A.; Li, R.; Tancik, M.; Li, H.; Ng, R.; and Kanazawa, A. 2021. Plenotrees for real-time rendering of neural radiance fields. In *ICCV*, 5752–5761.
- Zhang, K.; Riegler, G.; Snavely, N.; and Koltun, V. 2020. Nerf++: Analyzing and improving neural radiance fields. *arXiv preprint arXiv:2010.07492*.
- Zhang, X.; Srinivasan, P. P.; Deng, B.; Debevec, P.; Freeman, W. T.; and Barron, J. T. 2021. NeRFactor: Neural Factorization of Shape and Reflectance Under an Unknown Illumination. *arXiv preprint arXiv:2106.01970*.
- Zhou, Y.; Zhu, Z.; Bai, X.; Lischinski, D.; Cohen-Or, D.; and Huang, H. 2018. Non-stationary texture synthesis by adversarial expansion. *ACM Trans. Graph.*, 37(4): 49.